

Supporting Information

P3HT-Based Visible-Light Organic Photodetectors Using PEI/PAA Multilayers as a p-Type Buffer Layer

*Chan Hyuk Ji, Seon Ju Lee and Se Young Oh**

Department of Chemical and Biomolecular Engineering, Sogang University, Seoul 04107,
Republic of Korea

Table S1 Thickness and RMS surface roughness according to the number of PEI/PAA bilayers.

	Thickness (nm)	RMS (nm)
ITO	135.8±0.3	4.4±0.3
ITO/(PEI/PAA) ₁	3.3±0.1	3.5±0.2
ITO/(PEI/PAA) ₂	7.4±0.4	1.4±0.2
ITO/(PEI/PAA) ₃	12.2±0.9	1.4±0.1
ITO/(PEI/PAA) ₄	19.4±0.2	1.4±0.1

Table S2 Comparison of P3HT-based photodetector with similar structure.

Structure	Responsivity (A/W)	Dark current density (A/cm ²)	D * (Jones)	Reference
ITO/(PEI/PAA)₂/P3HT:PC₆₀BM/Yb/Al (at 525 nm, -1 V)	0.304	2.99 x 10 ⁻⁸	3.11 x 10 ¹²	This work
ITO/PEIE/P3HT:PC₆₀BM/Al (at 550 nm, -1 V)	14.25	2.77 x 10 ⁻⁶	1.04 x 10 ¹²	[49]
ITO/PEDOT:PSS/P3HT:PC₆₀BM/LiF/Al (at 530 nm, -1 V)	0.17	3.6 x 10 ⁻⁷	3.15 x 10 ¹¹	[12]
ITO/PEDOT:PSS/PbS: P3HT:PC₆₀BM:ZnO/Al (at 500nm, -4V)	5.6	≈ 2 x 10 ⁻⁵	1.01 x 10 ¹²	[51]
PEN/Ag/P3HT:PC₆₀BM/PEDOT:PSS (at 525nm, 0.9V)	≈ 0.66	≈ 2 x 10 ⁻⁷	1.5 x 10 ¹²	[52]
PEN/PEDOT:PSS/PEI/P3HT:PC₆₀BM/poly-PT/PEDOT:PSS (at 505 nm, -0.1V)	≈ 0.3	7.5 x 10 ⁻⁸	2.2 x 10 ¹²	[53]

* ≈ is calculation value.

Reference

- [49] Y. Wang, L. Zhu, Y. Hu, Z. Deng, Z. Lou, Y. Hou and F. Teng, *Opt. Express*, 2017, **25**, 7719.
- [12] B. Arredondo, B. Romero, J. M. S. Pena, A. Fernández-Pacheco, E. Alonso, R. Vergaz and C. de Sios, *Sensors*, 2013, **13**, 12266
- [51] R. Dong, C. Bi, Q. Dong, F. Guo, Y. Yuan, Y. Fang and J. Huang, *Adv. Opt. Mater.*, 2014, **2**, 549.
- [52] G. Azzellino, A. Grimoldi, M. Binda, M. Caironi, D. Natali and M. Sampietro, *Adv. Mater.*, 2013, **25**, 6829.
- [53] A. Grimoldi, L. Colella, L. L. Monaca, G. Azzellino, M. Caironi, C. Bertarelli, D. Natali and M. Sampietro, *Org. Electron.*, 2016, **36**, 29.

Table S3 Electrical parameters calculated from impedance values of OPDs (at light state, -1V).

		PEIE (7.5nm)	(PEI/PAA) ₂ (7.4nm)
R ₁ (Ω)		20 (ITO sheet resistance)	
C ₁ (F)	Light	2.51×10 ⁻⁹	2.90×10 ⁻⁹
R ₂ (Ω)	Light	1.52×10 ³	5.70×10 ²

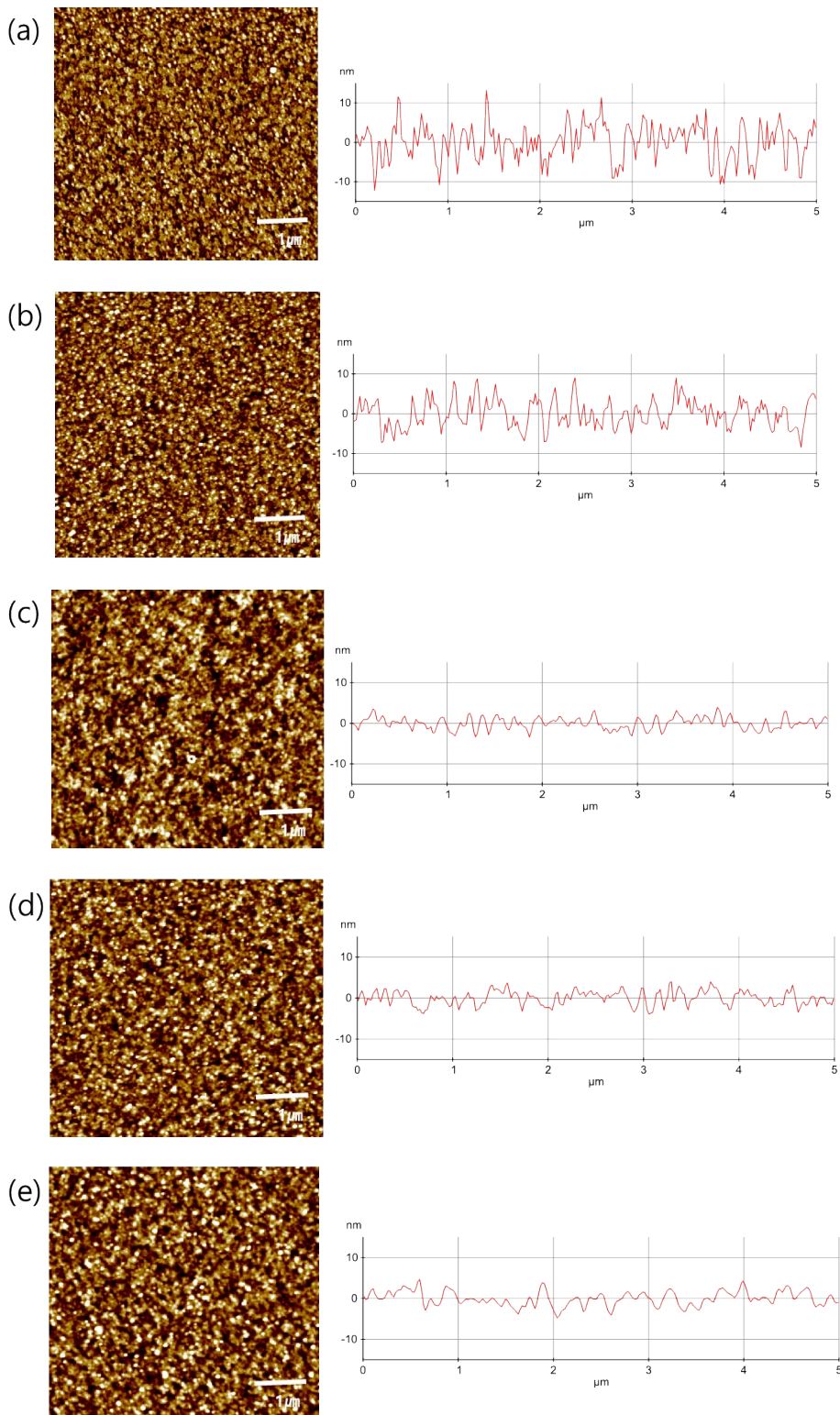


Fig. S1 AFM images of (a) bare ITO, (b) ITO/(PEI/PAA)₁, (c) ITO/(PEI/PAA)₂, (d) ITO/(PEI/PAA)₃, and (b) ITO/(PEI/PAA)₄ surfaces. Graphs on the right side show the corresponding section images of the center position.

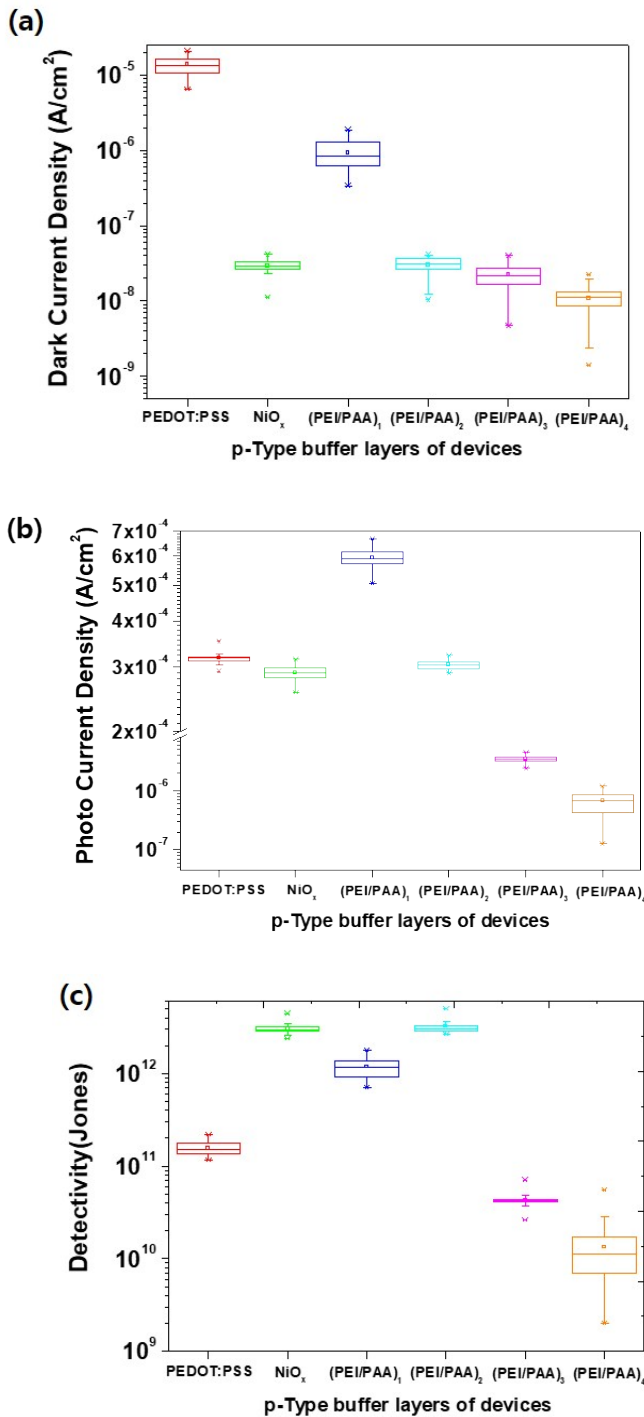


Fig. S2 Device statistics for (a) dark current density, (b) photocurrent density (at 525 nm, -1 V), and (c) detectivity of OPDs comprising different p-type buffer layers. The standard box plots represent the standard deviations (90% of all data points lie between the upper and lower whiskers).

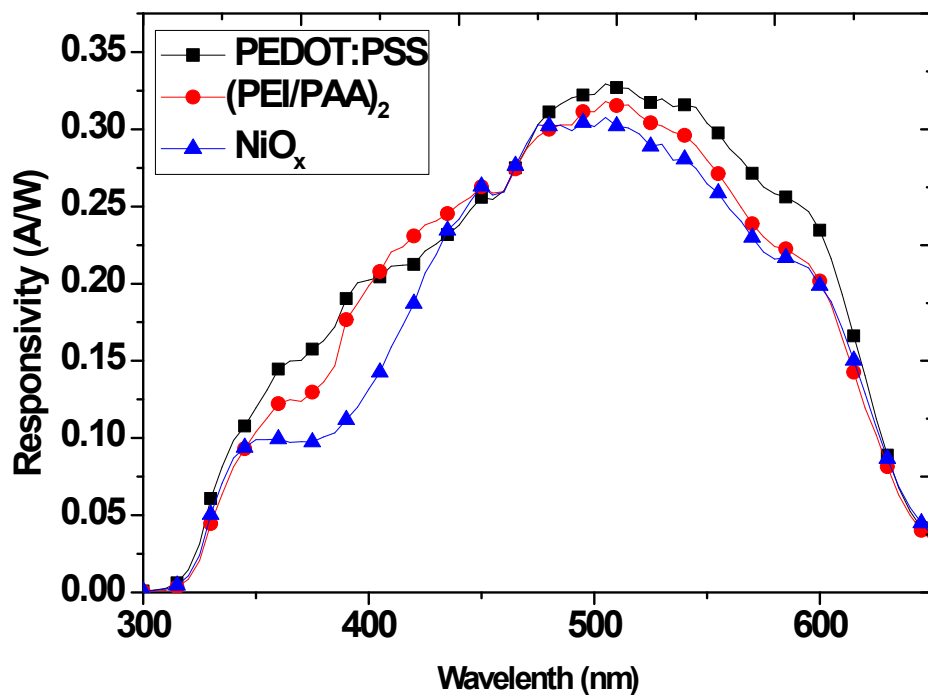


Fig. S3 Responsivities of OPDs comprising different p-type buffer layers at different wavelengths (1 mW/cm^2).

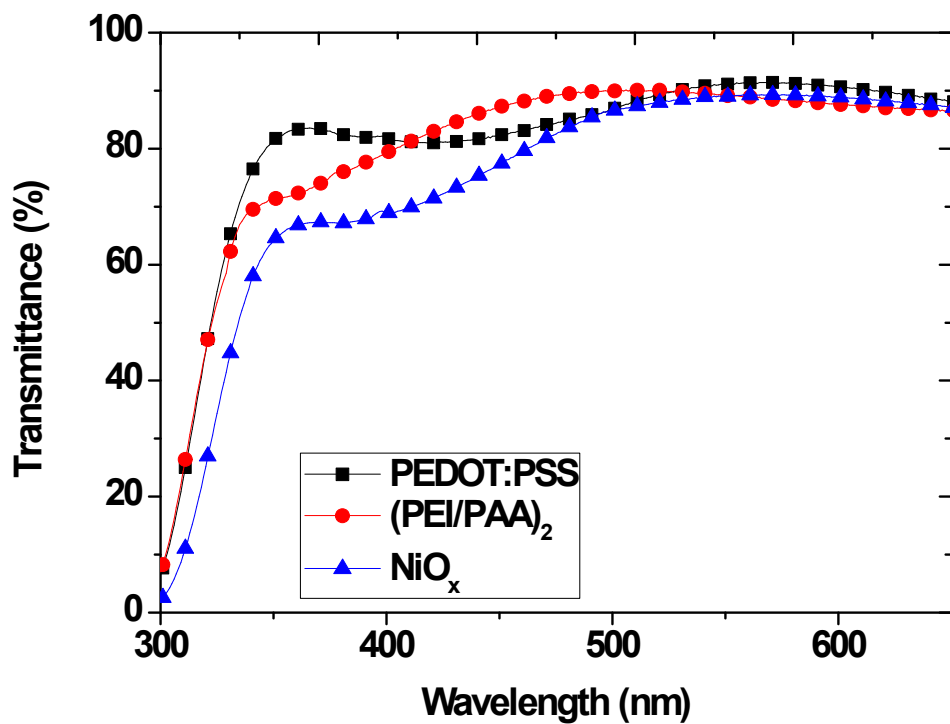


Fig. S4 Transmittances of p-type buffer layers on glass/ITO substrates.

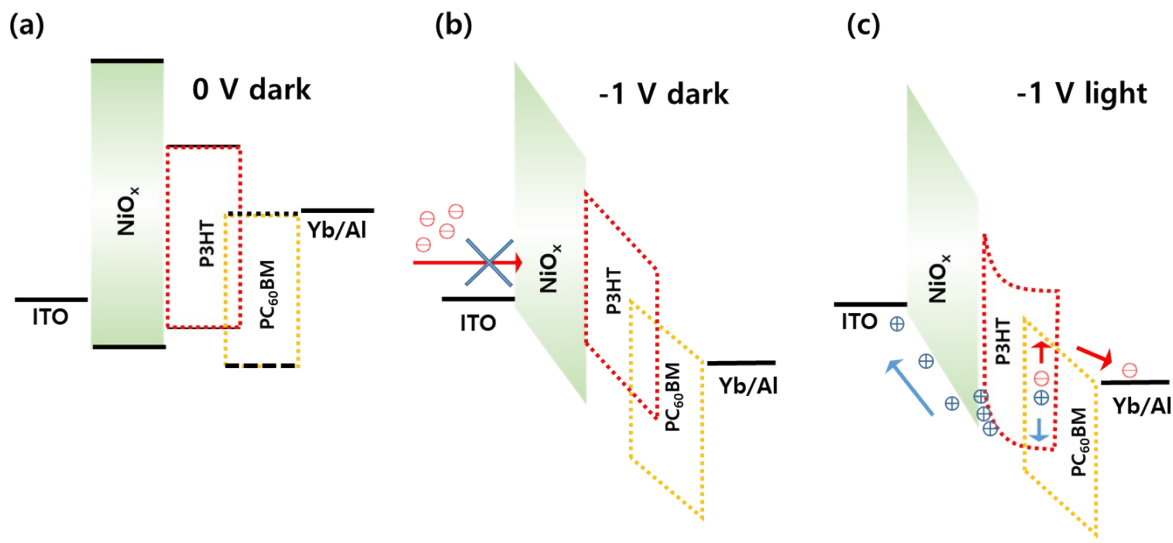


Fig. S5 Carrier transport mechanism of the device using NiO_x . (a) 0 V, dark state; (b) -1 V, dark state; and (c) -1 V, light state.

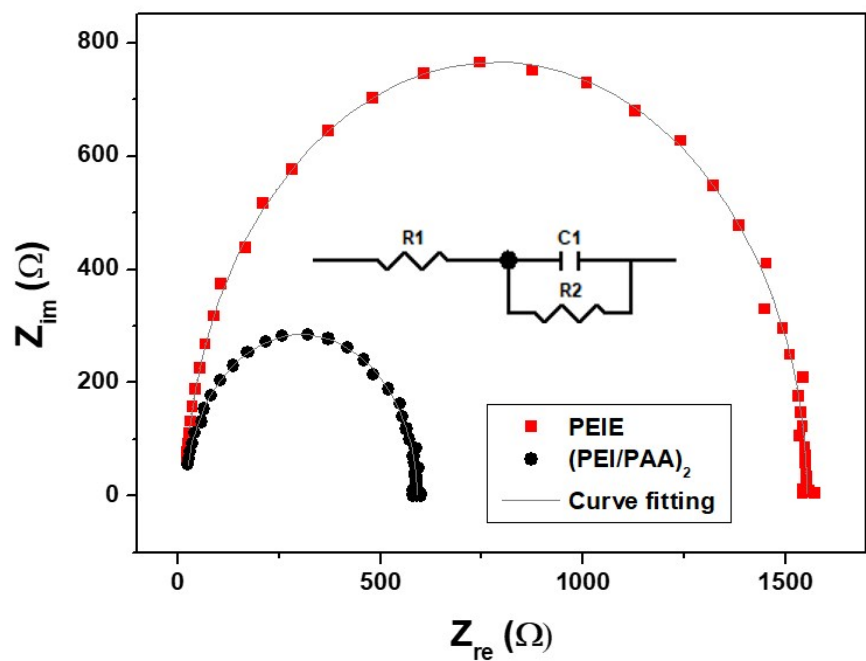


Fig. S6 Impedance spectra measured under light condition at 525 nm, -1 V and 1 mW/cm². The inset shows the equivalent circuit used to model the impedance.

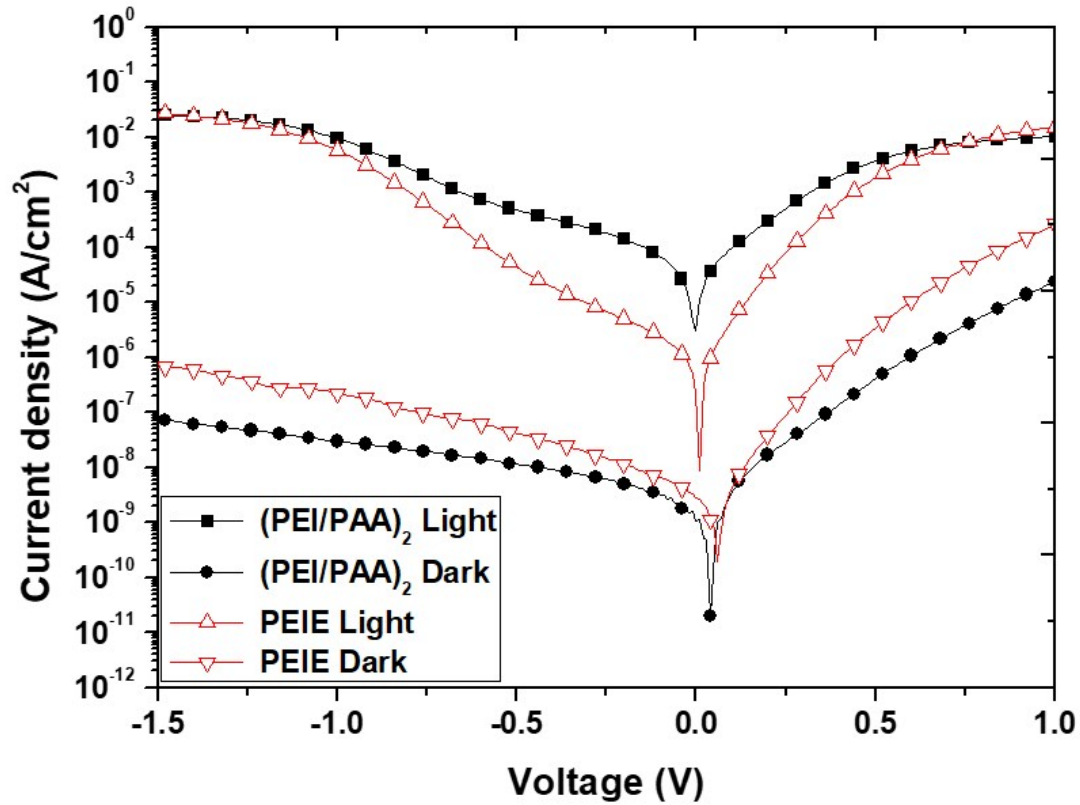


Fig. S7 Logarithmic J–V characteristics of OPDs at light (1sun) and dark state.

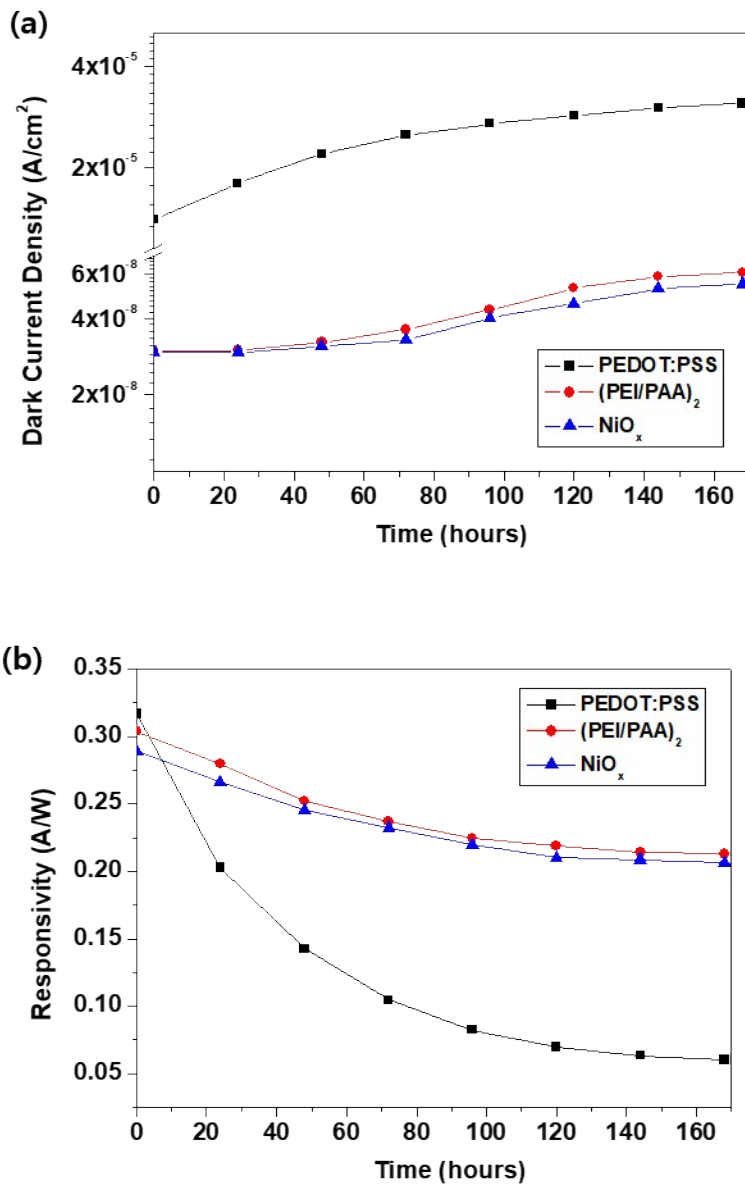


Fig. S8 (a) Dark current densities and (b) responsivities of OPDs over 168 h (7 days) after fabrication.

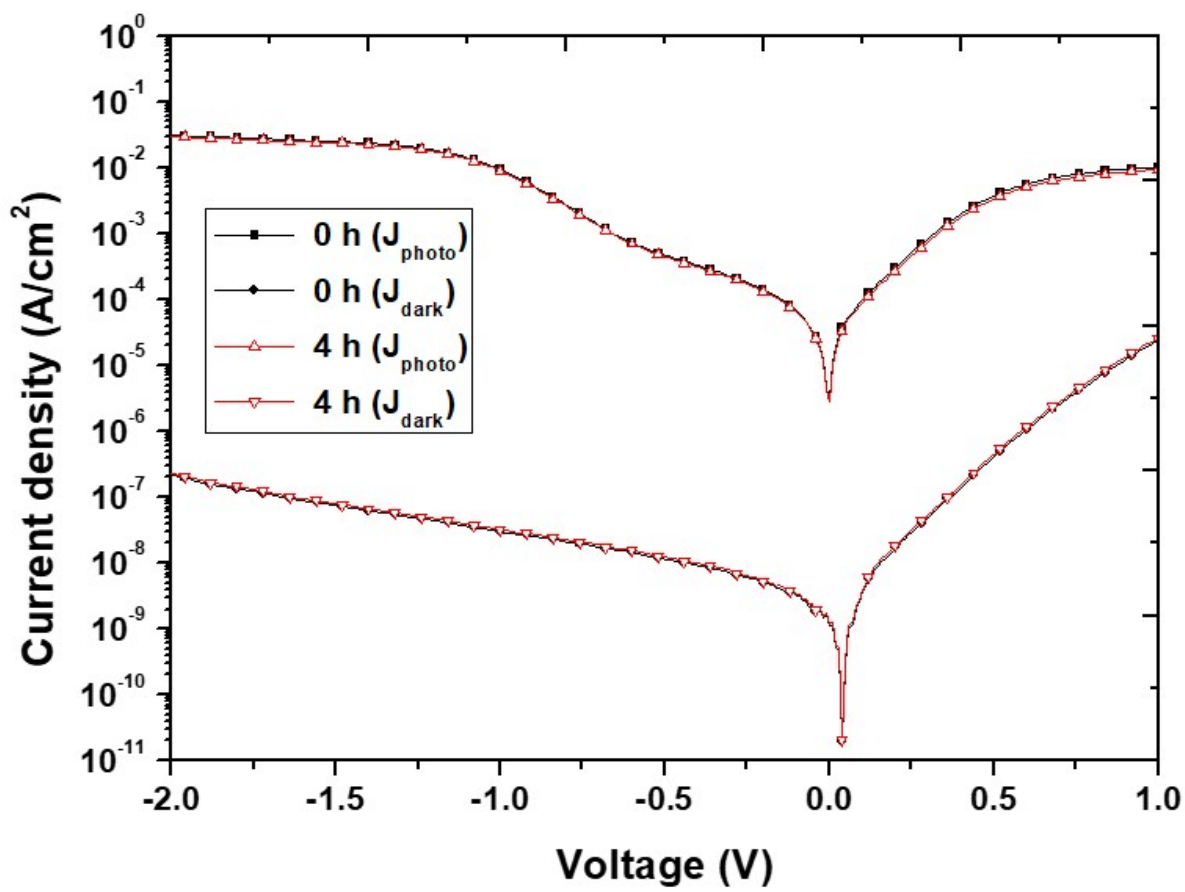


Fig. S9 Logarithmic J–V characteristics of the device using $(\text{PEI}/\text{PAA})_2$ at light (1sun) and dark state with 1sun irradiation time.